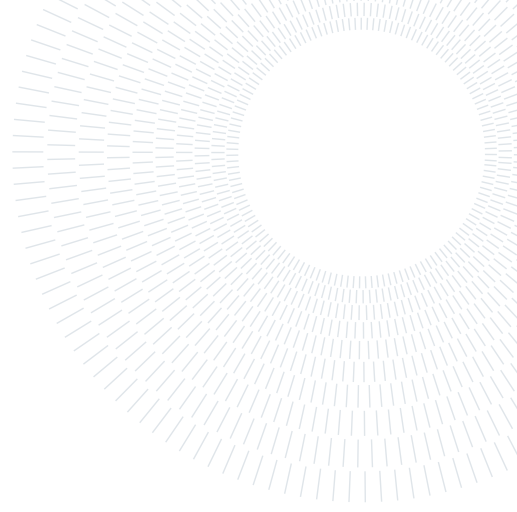




POLITECNICO
MILANO 1863

**SCUOLA DI INGEGNERIA INDUSTRIALE
E DELL'INFORMAZIONE**



Orbital Mechanics Project ID 2336

MSc SPACE ENGINEERING

Valentina D'Annunzio, 10729511, 251608
Mirko Mascaretti, 10741197, 252469
Edoardo Nicolucci Balocco, 10705062, 253013
Samuele Orsenigo, 10735389, 252212

Academic year:
2023-2024

1. Introduction

In this report, we present the findings of our project in the orbital mechanics course. The project consists of two sections: the first part involves analysing an interplanetary exploration mission from Saturn to Mars, leveraging Jupiter to execute a fly-by manoeuvre. Our goal is to determine the optimal manoeuvre within a given temporal window. Meanwhile, the second assignment evaluates the impact of two perturbation forces on a planetary orbit. We illustrate the effects of J_2 and air drag disturbances on the orbit across varying time frames.

2. Interplanetary mission Explorer

2.1. Mission Presentation

The aim of the interplanetary mission is to carry out a preliminary analysis of a transfer with the following characteristics:

- | | |
|-------------------------------------|------------------------------|
| • Departure Planet: Saturn | Earliest departure: 1/1/2028 |
| • Powered gravity assist on Jupiter | |
| • Arrival Planet: Mars | Latest arrival: 1/1/2058 |

The main objective of the analysis is to optimize the trajectory and to minimize the cost in terms of Δv . The following assumption have been made throughout the study: the flyby is considered to be an impulsive manoeuvre and the initial heliocentric orbit of the spacecraft is equal to the one of the departure planet at departure time while the final heliocentric orbit where the spacecraft will arrive is equal to the one of the arrival planet at arrival time. Any sort of perturbation like aerodynamic drag, solar radiation pressure, J_2 effect or presence of other celestial bodies is totally neglected. The most important assumption we did in our research is designing our interplanetary trajectory as several arcs of orbits in the two body problem, matching conditions on the radius and the velocity with the boundaries: this is the Patched Conics Method.

2.2. Preliminary analysis

2.2.1 Synodic periods and reference velocity

The first constraint used to reduce the grid search area is applied using the synodic periods, the time it takes for an object to reappear in the same relative position with respect to another body. Since all planets have more or less circular orbits with low inclination around the Sun we calculated it considering just the difference in the true anomaly. The result is a repetition of the velocity cost every synodic period, due to the same planets configuration, and this lead to a smaller time window for every transfer, because now we can cut off some useless parts of it.

In addition we calculate with our Matlab code *direct_Sat_Mar_no flyby.m* the best Δv obtained by going directly from Saturn to Mars, without the fly-by at Jupiter. In this code the time window for the departure goes from 2028 to 2053, because we noticed that when we get the minimum cost, the time of flight (*Tof*) is not smaller than 5 years. So we eliminated the last years to let the spacecraft arrives on Mars before 2058. As we expected, this transfer is very similar to the Homann's one, which would have been the most efficient manoeuvre if the two planets' orbits had been exactly coplanar and circular. We chose to use the value we found as the maximum acceptable, because otherwise the fly-by itself would not be meaningful.

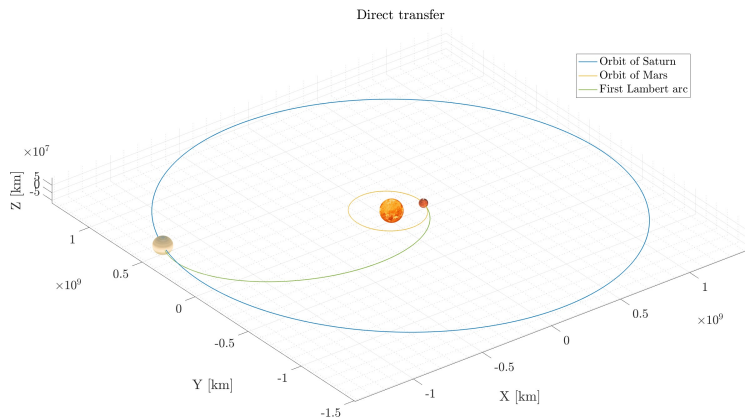


Figure 1: Direct transfer from Saturn to Mars

2.2.2 Saturn-Jupiter porkchop analysis

We can do a preliminary study by analysing the first Lambert arc between Saturn and Jupiter. To consider all the possible combinations we have to iterate all the possible departures times combining them with all the possible times of flight for this first part of the transfer. As we can deduce graphically from the pork chop plot there is one main area of interest that shows low velocity cost and it spans from 2028 to 2041 so we can replace the time span of departure with this one, further decreasing it. We can also observe a minimum and maximum time required for the transfer, because outside this area the velocities increase by quite a lot. For this reason we can impose that the ΔT for the first Lambert arc must be between 2000 and 6000 days.

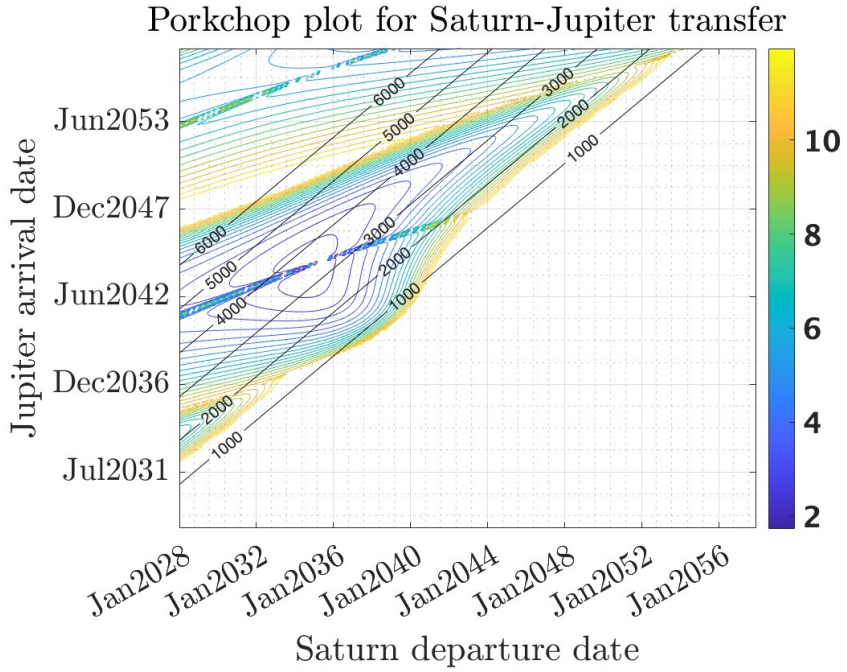


Figure 2: Porkchop plot of Saturn-Jupiter transfer

As mentioned before, the figure reveals a repetition pattern exactly every Jupiter-Saturn synodic period. However since their respective synodic period is 19.85 years there is only one region of minimum, if the area of analysis is increased the same pattern would be repeated along the diagonal.

2.2.3 Jupiter-Mars pork chop analysis

The same study can be done on the second part of the transfer, the arc that starts from Jupiter and ends on Mars. From the pork chop plot we can see that there is not a specific time more suited for the arrival, however it can be observed that the regions that have lower cost are spaced uniformly along the diagonal with a periodicity that coincides with the mutual synodic period of Jupiter and Mars. This plot is especially important however, because it allows to establish the required ΔT for the second part of the transfer, which must be over 500 and under 3000 days, as we can see in Figure 3.

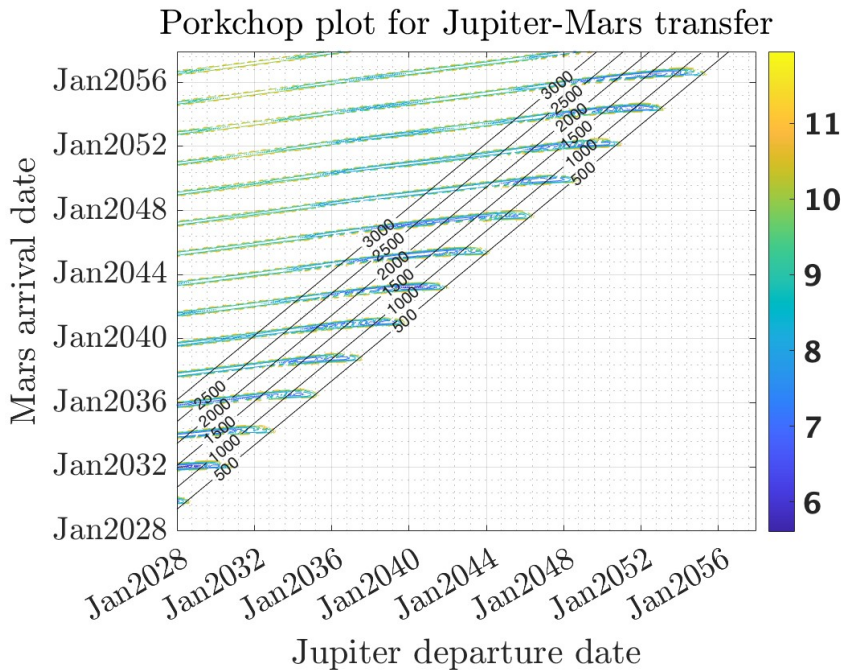


Figure 3: Porkchop plot of Jupiter-Mars transfer

As expected, the bigger constraint on time windows is originated from the first Lambert arc, because of the greater synodic period. So, for every possible arrival to Jupiter, only a few starting position from Saturn allow us to obtain a small transfer velocity, while for every arrival to Mars, there are multiple possible positions where Jupiter could be located without significant effect on transfer velocity.

2.2.4 Fly-By on Jupiter

The fly-by has a crucial role in this interplanetary transfer: it allows the spacecraft to save a decent amount of fuel to perform a change of orbit, exploiting the gravitational force of the planet.

The last constraint that we used in this part of our study was to set the minimum radius of pericenter where the powered gravity assist is performed. This value is equal to the radius of Jupiter, 69911 km, to which we add an altitude of 1000 km, for a total rounded up radius of 71000 km, because under that we would also have to consider the effects of aerodynamic drag.

2.3. Grid research algorithm

Once defined the time areas that we are going to search we can use the function *grid_search* to find the minimum Δv needed to perform the mission. The function utilises three inputs: the time span for departure time and the time spans for the time of flight of the first and second Lambert's arc. The time it takes to reach Jupiter from Saturn is longer than the time of flight from Jupiter to Mars, this has been accounted by discretizing the time spans differently according to their width. To improve the time of iteration during the cycle a restraint has been placed on the Δv of each Lambert's arc to exclude velocities over a certain value and skip that iteration. Furthermore if the radius of the flyby is too low, then the spacecraft would not be able to perform the powered gravity assist so a constraint has been placed to exclude flybys where the radius of pericenter is not acceptable.

2.4. Results

After the first grid search, for the time span decided above these are the results we find presented in Table 1:

Departure date	18/11/2034, 7 h, 53 m, 17.2 s
Tof of first Lambert	6.931 years
Flyby date	23/10/2041, 23 h, 38 m, 37.8 s
Tof of second Labert	3.623 years
Arrival date	8/6/2045, 6 h, 40 m, 47.9 s
Total cost [Km/s]	8.3716
Cost of first Lambert [Km/s]	2.3190
Cost of second Lambert [Km/s]	6.0498
Cost of the flyby [Km/s]	0.0028

Table 1: Solution after one grid search

This result can be further improved by reducing the length of the time span in order to get finer steps and a more accurate result. These final refinements are obtained using different time spans: in the first case we opted for a time window of a year around the data returned from the first grid search, calculating the planet's positions every week, except for Mars position which we calculated every day; in the second case we opted for a time window of two months around the data returned from the previous grid search, with a time span of a day, to be as precise as possible. The result we find are reported in Table 2.

As we can see the part of the mission with the major cost is the final impulse once the spacecraft arrives on Mars, it corresponds to the 72.36 of the total cost. The flyby, on the other side, has a really small impact as it happens quite far from the planet.

Departure date	7/1/2035, 7 h, 53 m, 17.2 s
Tof of first Lambert	6.822 years
Flyby date	2/11/2041, 23 h, 38 m, 37.8 s
Tof of second Lambert	3.596 years
Arrival date	8/6/2045, 6 h, 40 m, 47.9 s
Total cost [Km/s]	8.3681
Cost of first Lambert [Km/s]	2.3126
Cost of second Lambert [Km/s]	6.0554
Cost of the flyby [Km/s]	1.1072e-04

Table 2: Refined solution

2.4.1 Graphic results

The graphic results are here presented.

It is interesting to notice the time the spacecraft spends in the SOI of Jupiter during the flyby. The SOI of Jupiter is the region where the effects of the orbit perturbations due to Jupiter are stronger than the Sun's ones, and it's calculated as: $r_{\text{SOI}} \approx a \left(\frac{m}{M} \right)^{2/5}$, where a is the orbital radius of Jupiter, m is the mass of Jupiter and M is the mass of the Sun. The time spent in this region is 1.678×10^7 s, or more than 194 days, because of Jupiter mass.

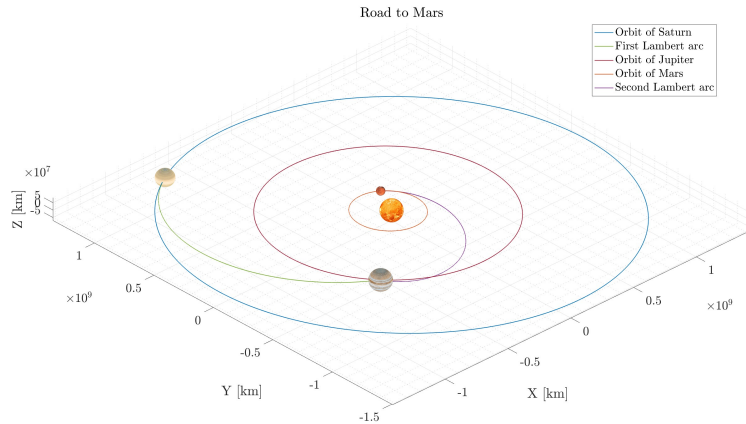


Figure 4: Heliocentric trajectories of the optimal solution

Radius of pericenter [Km]	1.1825e6
Tof in the SOI [days]	194
Δv given by the planet [Km/s]	7.4452
Powered Δv_p [Km/s]	1.1072e-4
Ratio between Δv_p and Δv	1.487e-5

Table 3: Flyby cost

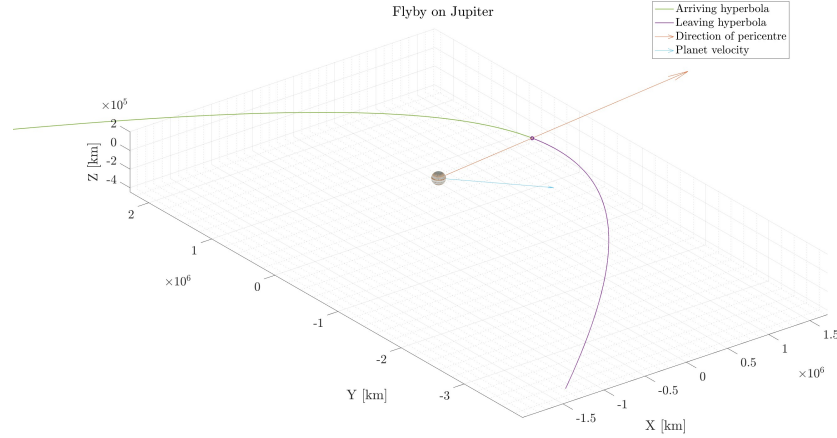


Figure 5: Flyby performed on Jupiter

2.4.2 Comparison with the Direct Transfer Manoeuvre

By comparing the result we just found with the ones returned by *direct_Sat_Mar_noflyby.m* that searches the best Δv of the direct transfer from Saturn to Mars without the fly-by in our time window, we can see how much it can be spared thanks to the fly-by. The Δv is about 11.9498 km/s , which is 142.8% bigger than the Δv with the Jupiter fly-by. So the saving of fuel is about 29.97%.

3. Planetary Explorer Mission

3.1. Mission Presentation

The primary objective of the assigned mission is to observe the progression of a designated orbit and provide a calculated estimation of the relative ground track. Moreover, we characterise the repeating ground track, modifying the semi-major axis to guarantee better communications with the network of ground stations. The assessment focuses solely on the influence of J2 and atmospheric drag perturbations, assuming negligible the impact from other ones. To track the evolution of the perturbed orbit over time, two propagation methods were employed and compared: Direct Cartesian coordinate propagation and Gauss' planetary equations propagation. To authenticate the accuracy of these propagation methods, we conducted a validation by comparing them with a real-case scenario using NASA Horizon propagation from ephemerides. This process involved seeking a case within the same orbital region and similar initial values, taken from the Space-Track catalogue.

3.2. Nominal Orbit Characterization and Perturbations models

The problem is initiated by the selection and description of the designated orbit, followed by the expression of the perturbation models employed in our work. The parameters given for the project are detailed in Table 4.

Table 4: Assigned data

a [10^4 Km]	e [-]	i [deg]	Repeating GT ratio k:m	Perturbations	Parameters	
0.6846	0.0298	80.2068	15:1	J2 DRAG	CD = 2.1	A/M = 0.0043 m^2/kg

3.2.1 Orbit selection and description

To fully define the initial orbit we need to select Ω , ω and θ . The missing elements were chosen, with some approximations, to be the same as DANDE DEB (LAB), a space debris that we take as a reference in the last part of our report. For simplicity, we set the initial θ as zero, to better discuss the result.

Ω [deg]	ω [deg]	θ [deg]
285	135	0

Table 5: Chosen orbital data

The orbit is a prograde quite-circular LEO orbit, with a polar inclination. The perigee is 271 km above the sea, which means that the satellite will be affected by drag and it will eventually decay. The period of the orbit is 93 minutes and 57 seconds.

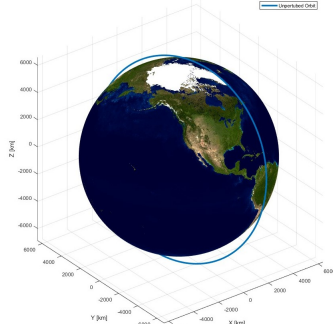


Figure 6: Unperturbed orbit

3.2.2 Perturbations models

J2 perturbation

For many applications (HEO, MEO) the most influential term of the gravitational perturbation is the contribution of the zonal harmonic potential J_2 , that takes into account the Earth's oblateness. This perturbation can be expressed (in ECI Equatorial reference frame) through the equation:

$$\mathbf{a}_{J_2} = \frac{3}{2} \frac{J_2 \mu R_\oplus^2}{r^4} \left[\frac{x}{r} \left(5 \frac{z^2}{r^2} - 1 \right) \hat{\mathbf{i}} + \frac{y}{r} \left(5 \frac{z^2}{r^2} - 1 \right) \hat{\mathbf{j}} + \frac{z}{r} \left(5 \frac{z^2}{r^2} - 3 \right) \hat{\mathbf{k}} \right] \quad (1)$$

where R_\oplus is the Earth's equatorial radius, $J_2 = 0.00108263$ is a constant coefficient and $\mathbf{r} = x\hat{\mathbf{i}} + y\hat{\mathbf{j}} + z\hat{\mathbf{k}}$ is the position vector of the satellite expressed in the ECI Equatorial reference frame. From the theory we know that the principal effect of the J_2 perturbation is the Nodal regression which is a change in the value of the Right Ascension of the Ascenting Node (RAAN), causing a rotation of the orbital plane. In this case, having an orbit with initial inclination of 80.2068° , the orbital plane will rotate towards West over time, as shown in Fig.11.

The J_2 perturbation also affects the Argument of the pericenter and the True anomaly. A more in-depth study on their variation over time is provided in paragraph 3.4.

Air drag perturbation

The atmospheric drag is a non conservative force that can be modeled as:

$$\mathbf{a}_{\text{drag}} = -\frac{1}{2}\rho \frac{A}{m} C_d v_{\text{rel}}^2 \frac{\mathbf{v}_{\text{rel}}}{\|\mathbf{v}_{\text{rel}}\|} \quad (2)$$

with ρ the atmospheric density, A the cross sectional area, m the spacecraft mass, C_d the drag coefficient and v_{rel} the spacecraft velocity relative to the atmosphere $\mathbf{v}_{\text{rel}} = \mathbf{v}_{\text{SC}} - \omega_{\oplus} \times \mathbf{r}_{\text{SC}}$, where $\omega_{\oplus} = [0, 0, 7.2921 \cdot 10^{-5}]^T \text{rad/s}$ is the Earth's rotational speed and \mathbf{v}_{SC} and \mathbf{r}_{SC} denote respectively the velocity and position of the spacecraft in the Earth-Centered Inertial (ECI) frame.

Behind this simple formulation lies a model fraught with uncertainty in determining all its parameters. In fact, the most challenging aspect is defining the density. These equations are built on the assumption of a time-independent, spherically-symmetric atmosphere with a density that varies exponentially with altitude h , according to an exponential law [3]. Within this context, we have disregarded the impact of wind and have not accounted for temperature variations throughout the day. Furthermore, we have not considered the satellite's orientation, which could affect the assumption of a constant $C_d = 2.1$ and $\frac{A}{m} = 0.0043 \text{m}^2/\text{kg}$.

3.3. Ground track

The ground track is the projection of a satellite's orbit onto the Earth's surface. In this assignment the ground track is computed for both the unperturbed and perturbed orbits over two time spans: one orbital period and one day, as shown in Fig.7.

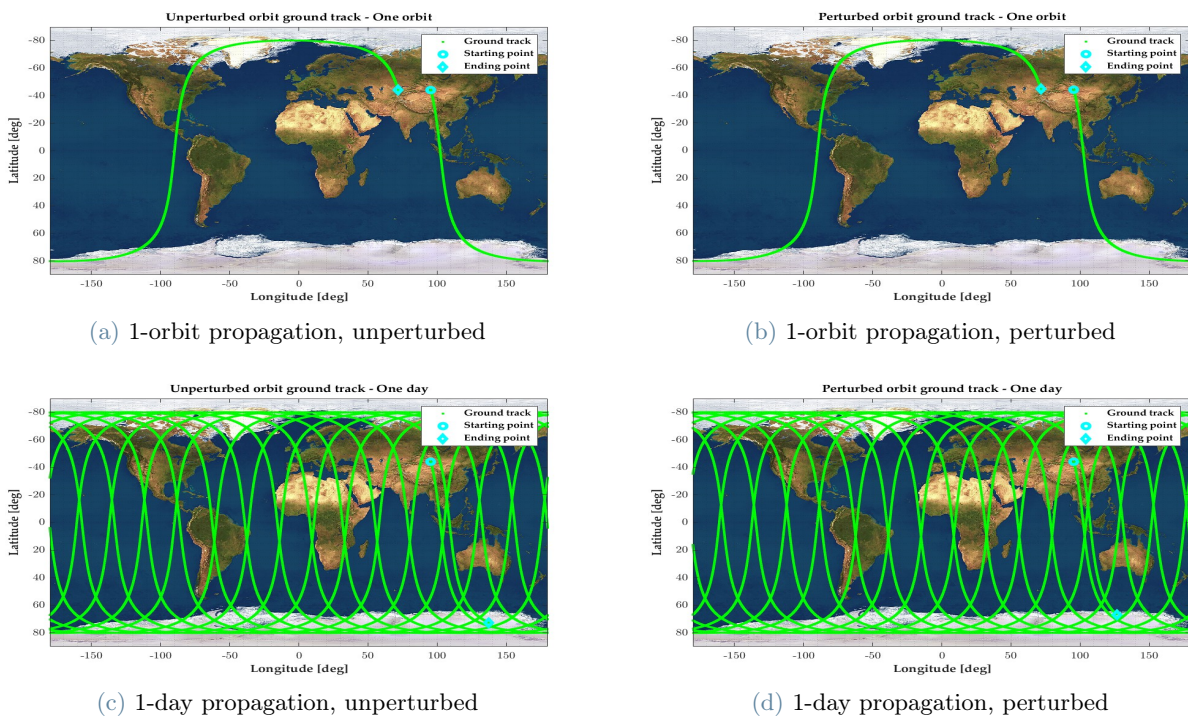


Figure 7: Ground tracks for unperturbed and perturbed cases

It is interesting to note that the ground track changes with the variation of the orbital elements Ω , ω and θ .

- In Fig.8(a) it can be seen that different values of Ω simply cause a shift in the longitude of the starting point, maintaining the same value of its latitude, due to the rotation on the Nodal line only around the Z axis of the ECI Equatorial reference frame;
- Fig.8(b) shows the ground track for two different values of ω . Here the starting point changes in both its longitude and latitude, following the rotation of the perifocal frame with respect to the ECI Equatorial frame. The change of the ground track's shape cannot be seen because the orbit is almost circular ($e = 0.0298$);
- different values of θ modify the initial longitude and latitude of the satellite, as shown in Fig.8(c).

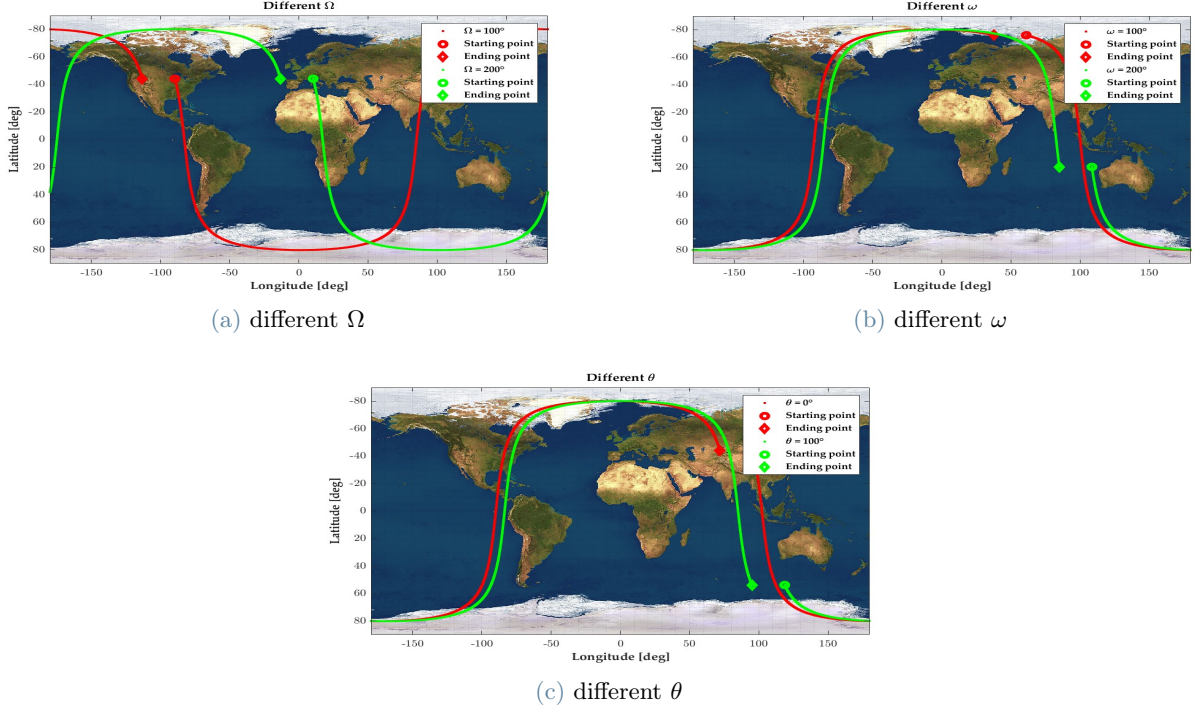


Figure 8: Ground tracks with modified keplerian elements

3.3.1 Repeating ground track

It is possible to obtain a repeating ground track for the unperturbed orbit by modifying its semi-major axis using the following equation:

$$a_{rep} = \sqrt[3]{\mu \left(\frac{m}{k\omega_{\oplus}} \right)^2} \quad (3)$$

where k is the number of revolutions of the satellite and m is the rotation of the Earth, their values are shown in Table 6.

Table 6: Repeating parameters

k [-]	m [-]
15	1

From the figure below, it can be seen that there is no issue with the repeating ground track of the unperturbed orbit, because the starting and the ending point coincide.

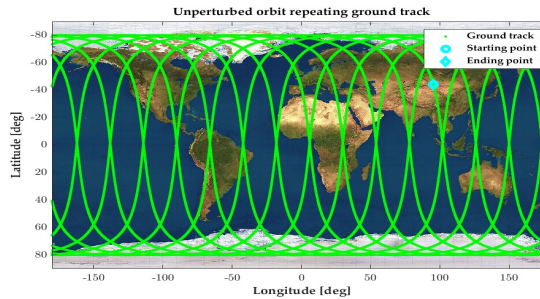


Figure 9: Repeating ground track for the unperturbed orbit

On the other hand, for the perturbed case, the repeating ground track is not possible with the new value of the semi-major axis, due to the modification of the keplerian elements caused by the perturbations. In Fig.10 it is shown the repeating ground track with semi-major axis equal to a_{rep} and a zoom-in of the error, for the perturbed case. This error is caused by:

- the decay of the semi-major axis, due to the atmospheric drag. The decay causes the decreasing of the orbital period and the satellite crosses again over the Equator in less time, causing a eastward shift in the ground track;
- the nodal regression, due to the J_2 perturbation. This causes a rotation of the orbital plane, as above-mentioned in paragraph 3.2.2.

In order to obtain a repeating ground track for the perturbed case too, periodic orbit corrections must be made [2].

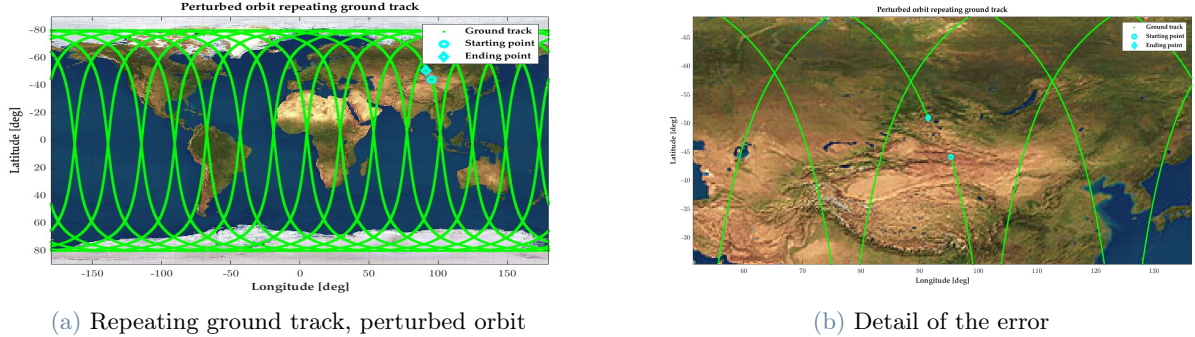


Figure 10: Repeating ground track for the perturbed orbit (J_2 and air drag perturbations)

3.4. Orbit Propagation

In this section, we will showcase the results of the propagated model. We integrated the problem using the function *ode113*, a multi-step ODE solver to achieve high accuracy. We compare two methods: one utilizes equations in Cartesian coordinates, while the other employs the Gauss' equations in RSW (radial-transversal-out-of-plane). To better illustrate our findings, we present the solution across different time frames: the short-term effects, where we observe the most variations, the long-term and secular effects and lastly, the end-of-life prediction for our satellite.

3.4.1 Short-term analysis

We have conducted a brief analysis to observe the impact of two accelerations along the orbit. To better examine the short-term effects, we have set the time frame to 2 orbital periods. As shown in Fig.12, the drag effect is most noticeable at the pericenter and least noticeable at the apocenter. On the other hand, the effect of J_2 is more complex and manifests in various ways with varying intensities throughout the orbit.

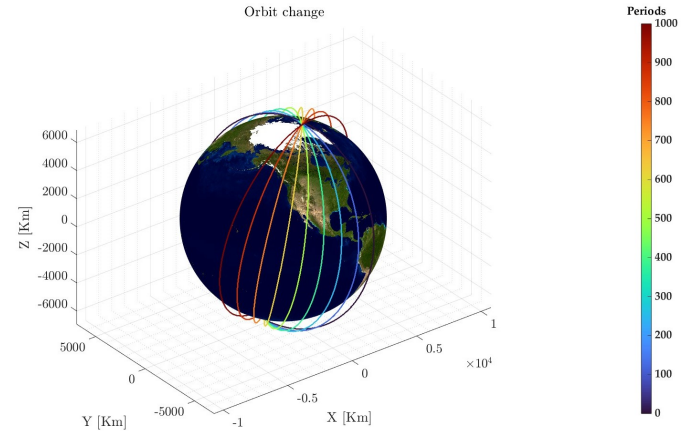


Figure 11: Movie of change orbit

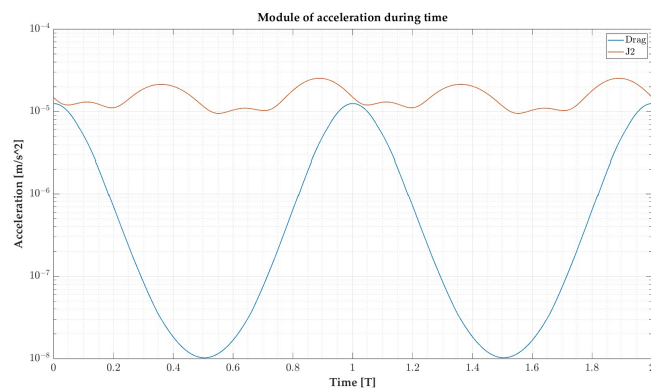


Figure 12: Acceleration

In the next figures, we have compared the results obtained from the Cartesian and Gauss methods, as well as the individual effects of drag and J2 as the only disturbance. The magnitude of acceleration attributed to J2 is notably higher throughout the orbit, significantly influencing the solution. The integration of J2 is closely aligned with the fully integrated problem, as evident from the figure and zoomed details in the red rectangle. The values are very similar, and in the short term, the effect of J2 induces substantial variations across all Keplerian variables. Conversely, the sole influence of drag remains quite limited.

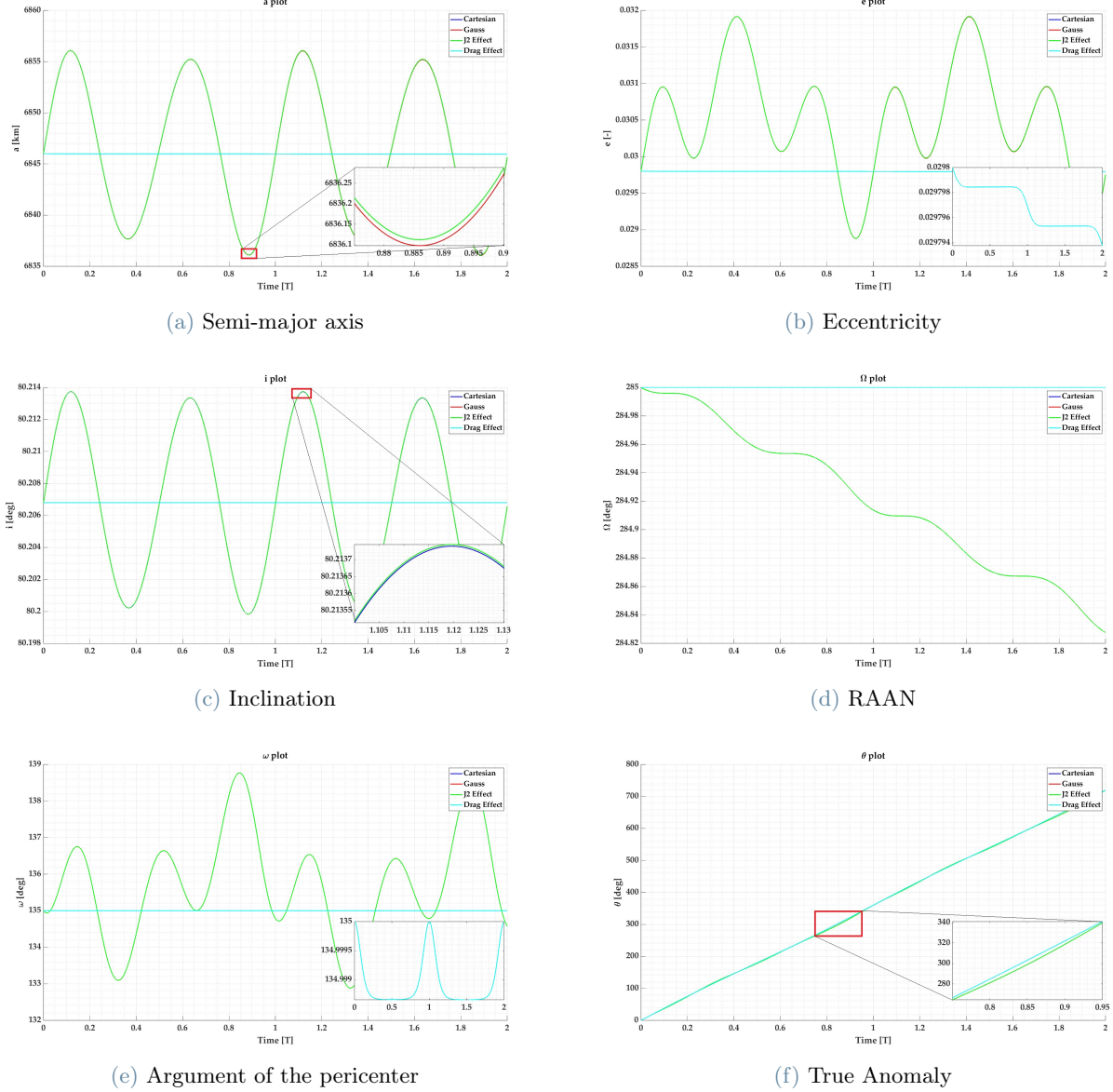


Figure 13: Short term analysis of keplerian elements

The drag can be modeled like an instantaneous manoeuvre at the pericenter. This is illustrated in Fig.13(b), where we observe the eccentricity variation resembling a step function, specifically near the pericenter (similar observations can be made for the semi-major axis).

3.4.2 Long-term and Secular analysis

We conducted multiple analyses to examine the changes in the orbital parameters over extended periods and determine a suitable time frame for the long-term and Secular analysis. After studying different time spans, we integrated within a period of 600 orbits, which roughly equals 40 days. In the next figures, we filtered the oscillations due to the short-period effect to obtain the secular effect. In this case, the long-term and secular effects are similar, and only eccentricity manifests a wide periodic change oscillation (see figure 14). We also compared the secular trend with theoretical secular trends of the solo disturbance. From theory, we know that J2 has secular influences on Ω and ω , while drag affects a and e (for more details see [2]). To model the variation

of the orbital parameters for each orbit we use:

$$\Delta\Omega_{j2} = \frac{-3\pi J_2 R_\oplus^2 \cos i}{a^2(1-e^2)^2} \quad \Delta\omega_{j2} = \frac{3\pi J_2 R_\oplus^2}{a^2(1-e^2)^2} \left(2 - \frac{5}{2} \sin i^2\right) \quad \Delta a_{drag} = -\frac{c_D A}{m} a^2 \int_0^{2\pi} \frac{\rho(r(E) - R_\oplus)(1+e \cos(E))^{3/2}}{\sqrt{1-e \cos(E)}} dE \quad (4)$$

Where E is the eccentric anomaly, an auxiliary variable to describe the orbit.

The "long term" filters are calculated using the matlab function *smooth* in order to better describe the true data, we use the option 'rloess' and we use a span of 30% of the total number of data points [1]. The 'true' secular filters are derived using the *movmean* function over a large interval to capture the trend effects. While these values may diverge from the theoretical ones (in cases involving J_2 or drag), they demonstrate similar behaviors."

As anticipated, the values for the semi-major axis and eccentricity diminish gradually due to aerodynamic drag, which tends to make the orbit more circular. J_2 primarily induces the orbital plane to precess. The Right Ascension of the Ascending Node (RAAN) at an inclination of 80° decreases, making the line of nodes shift westward. Also, the argument of the pericenter decreases, leading to the westward precession of the perigee.

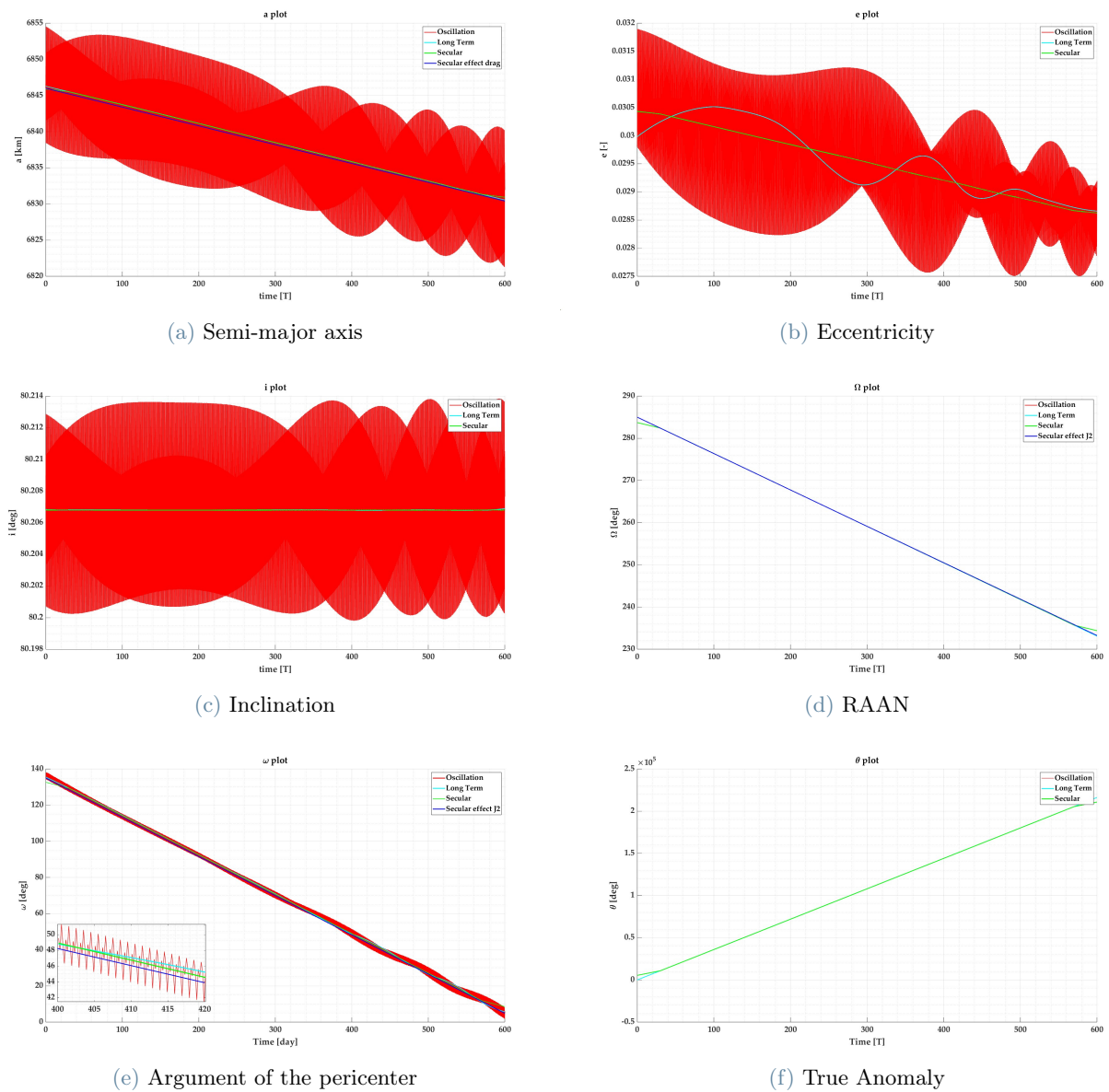


Figure 14: Long term analysis of keplerian elements

In Fig.15 we also present a logarithmic scale graph showing the relative errors between the Gauss method and the Cartesian one. As the propagation time increases, the two methods diverge increasingly.

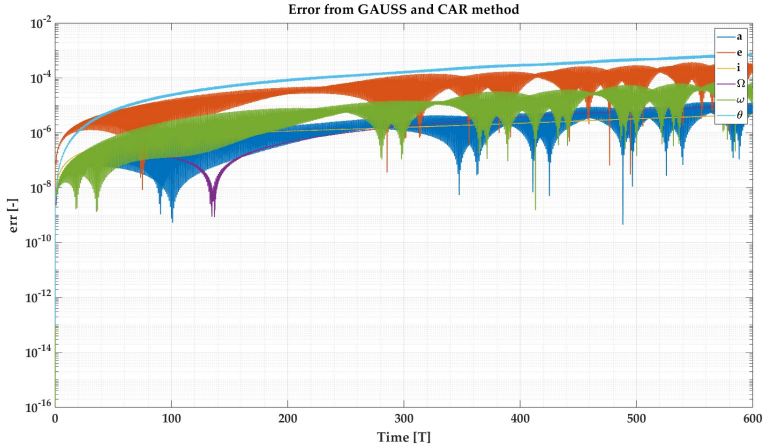


Figure 15: Relative error between Cartesian and Gauss

3.5. End-of-Life study

It can be of particular interest to forecast the satellite's reentry considering these perturbations. The simplest approach involves integrating the system with a lower limit constraint set at 100 km altitude (the altitude at which the satellite is considered deorbited). This method yields an estimated lifespan of approximately 305 days and 19 hours. For this calculation, we exclusively integrated the Cartesian model.

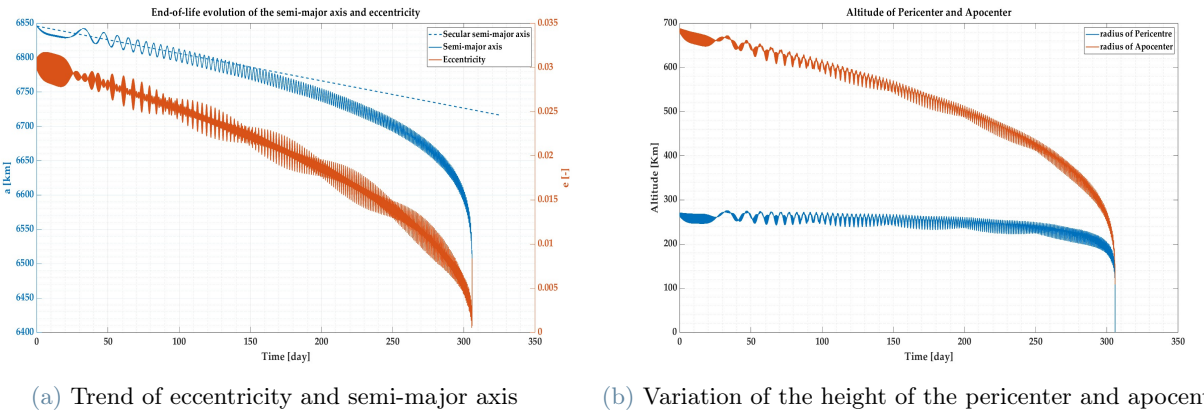


Figure 16: End-of-life analysis

This result is based on substantial simplifications, as it relies on an exponential density model and considers solely J2 and drag as a disturbance. Therefore, it can only offer a preliminary analysis that should be further explored in a real-world scenario.

3.6. Comparison with real data

In order to validate the model used to propagate the orbit in this assignment, a comparison with a real orbiting object has been made. The object is the DANDE DEB (LAB), a satellite debris, chosen due to its orbital elements similar to those of this assignment. A period of one month has been chosen to analyse the differences between real data and propagation, starting from 20/11/2023 to 21/12/2023.

Table 7: DANDE DEB (LAB) orbital elements on 2023/11/20 20:00:00

a [10^4 Km]	e [-]	i [deg]	Ω [deg]	ω [deg]	θ [deg]
0.68629	0.0298	80.8192	284.6658	135.5207	297.2336

The propagation model used for the comparison was the integration of Gauss' equations. The plots in Fig.17 show the filtered data for both the real keplerian elements and the propagated ones. It can be noted that the

semi-major axis, eccentricity, Ω and ω have all a downward evolution, although those of a and e decrease with different rate with respect to the real data. This can be explained by having neglected the other perturbations, even though they have small effects on orbital elements of LEO orbits. It is interesting to note, in Fig.17(c), how the real data of the inclination differ from the propagated ones. This is due to the fact that the air drag and J_2 perturbations used in our model do not affect the inclination.

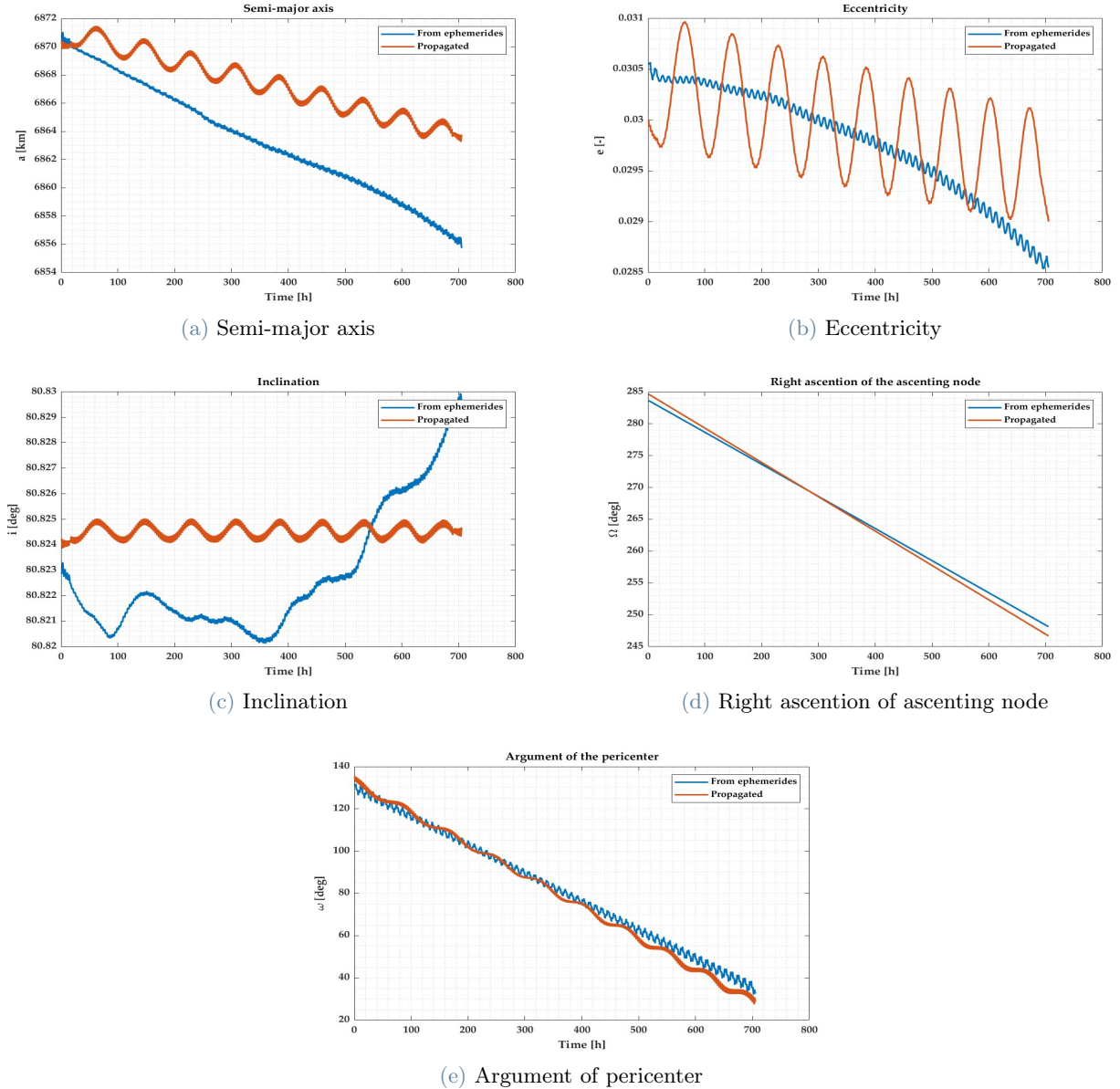


Figure 17: Comparison between the propagated elements and the real ones

3.7. Conclusions

The analysis of the planetary mission has shown that there are substantial differences between the unperturbed 2 body problem and the perturbed one. Just considering two (J_2 and air drag) of the many perturbations that affect the orbit, it can be seen that the propagation of the latter shows significant changes between the unperturbed and perturbed cases, due to the variation of the keplerian elements. Perturbations also affects the repeating ground track, which is no longer possible without proper orbit corrections. For future works, the team should be able to model other perturbations in order to obtain results closer to reality through the propagation methods.

References

- [1] Mathworks. <https://it.mathworks.com/help/curvefit/smooth.html>.
- [2] D.A. Vallado and W.D. McClain. *Fundamentals of Astrodynamics and Applications*. Fundamentals of Astrodynamics and Applications. Microcosm Press, 2001.
- [3] J.R. Wertz. *Spacecraft Attitude Determination and Control*. Astrophysics and Space Science Library. Springer Netherlands, 1978.